Targeted chitosan-based bionanocomposites for controlled oral mucosal delivery of chlorhexidine

Title: Targeted chitosan-based bionanocomposites for controlled oral mucosal delivery of chlorhexidine

Author: Renée Onnainty Barbara Onida Paulina Páez Marcela Longhi Antonello Barresi Gladys Granero

PII: S0378-5173(16)30487-2
DOI: http://dx.doi.org/doi:10.1016/j.ijpharm.2016.06.011
Reference: IJP 15819

To appear in: *International Journal of Pharmaceutics*

Received date: 22-2-2016
Revised date: 18-5-2016
Accepted date: 6-6-2016

Please cite this article as: Onnainty, Renée, Onida, Barbara, Páez, Paulina, Longhi, Marcela, Barresi, Antonello, Granero, Gladys, Targeted chitosan-based bionanocomposites for controlled oral mucosal delivery of chlorhexidine.International Journal of Pharmaceutics http://dx.doi.org/10.1016/j.ijpharm.2016.06.011

Targeted chitosan-based bionanocomposites for controlled oral mucosal delivery of chlorhexidine

Renée Onnainty [1], Barbara Onida [2], Paulina Páez [1], Marcela Longhi [1], Antonello Barresi [2], Gladys Granero [1]*

[1]Facultad de Ciencias Químicas, UNC-CONICET-UNITEFA

[2]Ciudad Universitaria, X5000-HUA, Córdoba, Argentina. Dipartimento di Scienza Applicata e Tecnologia, Politecnico di Torino; corso Duca degli Abruzzi 24, 10129 Torino, Italy

*E-mail: glagra@fcq.unc.edu.ar

Graphical abstract

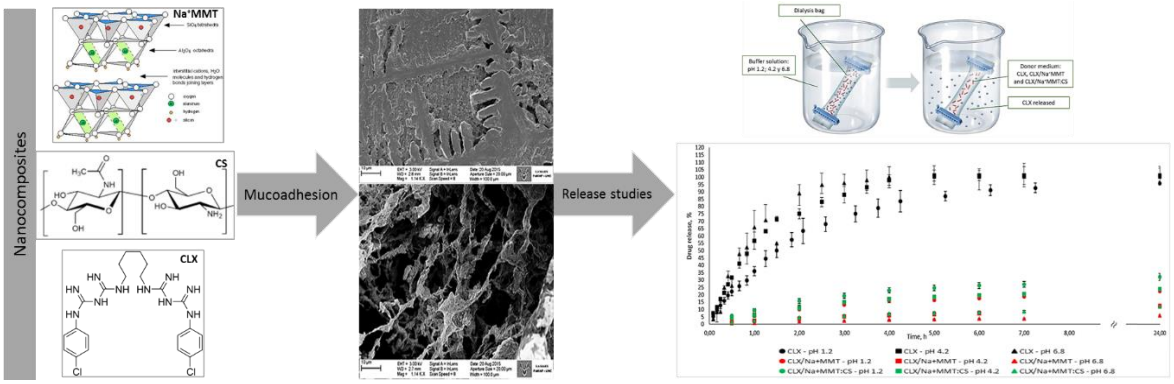

ABSTRACT. The purpose of this study was to develop sustained release systems based on chitosan (CS) and montmorillonite (MMT) for chlorhexidine (CLX). Nanocomposites were prepared by ion-exchange. CLX systems were characterized by X-ray powder diffraction (XRD), thermal analysis (TGA), Fourier transform infrared spectroscopy (FTIR), scanning electron microscopy (SEM) and X-ray fluorescence analysis (XRF). The mucoadhesion properties of CLX nanocomposites were evaluated by SEM. The release behavior of these systems was also studied by the dialysis technique. The antibacterial activity was investigated *in vitro* by the disk diffusion test. Results showed long-term sustained release of CLX from the hybrid carriers without initial burst release. The release profiles of CLX from the carriers suggested the diffusion through a swollen matrix and water filled pores as the controlled drug release mechanism. The CLX hybrid nanosystem containing the positively-charged chitosan exhibited good mucoadhesion properties maintaining the CLX antimicrobial properties.

Keywords: Chlorhexidine, Chitosan, Nanocomposites, Drug delivery systems, Mucoadhesion, Antibacterial activity.

1. Introduction

The development of antibacterial materials that could be utilized for medical purposes involves substances that can act as carriers of antimicrobials agents for local treatment. Topical therapy affords many potential advantages including the avoidance of the systemic effects of treatment. The local treatment of the oral cavity, however, has limitations as the relatively small surface area of the oral mucosa and the significant loss of drug due to uncontrolled swallowing and salivary flow of this route (Li & Robinson, 2005). The human oral mucosa is multistratified, non-keranized and the drug permeation across the buccal epithelium is believed to involve both transcellular and paracellular routes. Considering characteristics having the oral mucosa, it is desirable that delivery systems attempted for this route of administration include properties like biocompatibility, mucoadhesiveness and capability of sustained drug release to maintain therapeutic levels over an extended period of time (Aduba et al., 2013). These formulations, therefore, should adhere to the oral mucosa and stay in this place for an extended period of time to allow the treatment be effective (Sudhakar et al., 2006).

Nanocomposites obtained by the combination of clay minerals and biopolymers for pharmaceutical applications have attracted a great interest (Aguzzi et al., 2007, Viseras et al., 2008, Viseras et al., 2010 and Chiu et al., 2012). These hybrid materials can, in fact, combine the properties of both inorganic and organic components, such as swelling, water uptake, mechanical properties, thermal behavior, rheology and bioadhesion (Günister et al., 2007). Nanocomposites can be constituted of a lot of biopolymers and clay minerals, including montmorillonite (MMT) and chitosan (CS) nanocomposites, designed for biomedical applications (Ariga et al., 2012 and Besinis et al., 2015).

CS, a cationic polysaccharide, is able to easily intercalate via ionic exchange into the negatively charged MMT interlayers (Darder et al., 2003). CS is a suitable polymer for oral mucosal drug delivery due to its bioadhesive properties, proving an extended retention time on the oral mucosa. At physiological pH, its muchoadhesion is mainly due to electrostatic attraction with the negatively charged mucin, combined with contributions of hydrogen bonding and hydrophobic effects (São Pedro et al., 2009, Dos Satos Miranda Costa et al., 2014 and Xu et al., 2015). CS is a natural linear polymer obtained by alkaline deacetylation of chitin. Chemically, CS is a copolymer of glucosamine and N-acetlyl-glucosamine with one primary amino and two

free hydroxyl groups for each C6 building unit (Koukaras et al., 2012). MMT belongs to the smectite group minerals and has a layered structure. Polymers in the MMT dispersions interact with the clay according to their ionic or non-ionic characteristics (Fengwei Xie et al., 2013). CS-clay nanocomposites are capable of enhancing the thermal stability and mechanical properties of CS (Marroquin et al., 2013), retarding the swelling properties of the polymer. Moreover, MMT:CS nanocomposites could retard the CS matrix dissolution in acidic medium, resulting in slower drug release from the nanocomposite matrix (Dader et al., 2003).

Chlorhexidine (CLX) is a bisguanide antiseptic. It has a wide spectrum of bactericidal activity against Gram-positive and Gram-negative bacteria. It is also effective against some fungi and yeast, including *Candida*, and some viruses like HIV and HBV. CLX is commonly used in dental applications (Kolahi et al., 2006). A number of over-the counter and professionally administered CLX-based preparations are available in a variety of formulations and in range of strengths (Walsh et al., 2015), although, these CLX formulations usually provide short-term efficiency, requiring repeated applications to maintain antibacterial activity. In this context, appropriate release systems of CLX controlling the local drug delivery would reduce the number of applications and enhance the patient compliance.

The main objective of this work was to develop a drug release system for treatment of oral infections by the combination of MMT:CS composites as delivery systems of chlorhexidine digluconate (CLX). MMT:CS and CLX/ MMT:CS composite hydrogels were prepared by ion-exchange technique and characterized using X-ray diffraction (XRD), X-ray fluorescence spectroscopy (XRF), Fourier transform infrared spectroscopy (FTIR), thermal analysis (TGA) and scanning electron microscopy (SEM). The drug loaded composites were evaluated for *in vitro* release characteristics by the dialysis bag technique. Also, these systems were characterized for their mucoadhesive properties. In addition, the antimicrobial activity of the CLX obtained delivery systems was tested qualitatively by measuring zone of inhibition on agar plates.

2. Materials and methods

2.1. Materials

Chlorhexidine digluconate (CLX) was purchased from Todo Droga. Commercially available low molecular weight chitosan powder (MW ~ 50,000 – 190,000 Daltons; Sigma-Aldrich) was used. According to the producer data, its deacetylation degree DD was about 85 %. Commercially available montmorillonite (Sigma-Aldrich) with average particle size ca. 10-30 nm (the producer data) was used as a nano-filler. Pig gastric mucin (PGM) was sourced from Sigma (molecular weight it is not reported by the supplier, product code: M1778) and was used without further purification.

2.2 Preparation of biopolymer montmorillonite (MMT):chitosan (CS), chlorhexidine (CLX)/MMT and CLX-loaded clay polymer nanocomposites.

Nanocomposites were obtained using MMT and Na^+MMT. The Na^+MMT clay was obtained by dispersing the MMT in a 1M $NaNO_3$ solution, during 24 h under magnetic stirring at 25 ºC. To separate the Na^+MMT were used two cycles of centrifugation at 4000 rpm for 15 min. The samples were freezing and lyophilized to get the sample in solid state.

The sodium montmorillonite (Na^+MMT): chitosan (CS) nanocomposite particles were synthesized using a protocol proposed by Kaemkit et al., 2013. Chitosan solution was prepared by dissolving 2.04 g of low molecular weight CS in 100 ml of an 2% (v/v) aqueous acetic acid solution. The pH of the CS solution was adjusted to 4.9 with 1M NaOH in order to avoid any structural change of MMT. A quantity of 1.28 g of Na^+MMT was swelled in 50 ml of MilliQ water and placed in an ultrasonic bath for 1h. Na^+MMT:CS suspensions were obtained by adding CS to the aqueous solution of Na^+MMT using a peristaltic pump (KD Scientific) at the rate of about 50 ml/h under vigorous stirring, followed by stirring at 60 °C for 24 h. Then, the Na^+MMT:CS system was washed four times with distilled water. The Na^+MMT:CS biocomposite was separated from the water by centrifugation at 4000 rpm for 15 min and then obtain the solid by Lyophilization. The drug loaded composite was obtained by dispersing 0.5 g of the nanocomposite system Na^+MMT:CS or 0.5 g of Na^+MMT in 25 ml of 0.22 M CLX aqueous solution under stirring overnight at room temperature. The loaded nanocomposite was then separated from the aqueous suspension by centrifugation at 4000 rpm for 15 min. A schematic representation of nanocomposites synthesis is shown in Scheme 1.

To determine the free CLX during preparation of the CLX/Na^+MMT:CS and CLX/Na^+MMT carriers, the centrifuged solution was collected. The weight of free CLX ($W_{free\ CLX}$) in the solution was determined by UV-visible spectrophotometry (Agilent Technologies Cary 60 UV-Vis) using a wavelength of 255 nm. The CLX loading efficiency was calculated as follows:

$$\text{CLX loading efficiency (\%)} = 100 \times (W_{total\ CLX} - W_{free\ CLX})/W_{total\ CLX} \quad (1)$$

where $W_{total\ CLX}$ is the amount of added CLX.

2.4 Characterization of montmorillonite:chitosan nanocomposite

The interaction of CS and MMT was analyzed by Fourier transform infrared spectrometry (Spectrometry 5 SXC Nicolet FT-IR) using a KBr disc. The determination was carried out under a transmittance mode at 4000-450 cm^{-1}, resolution of 4 cm^{-1} and scan number of 64 time/sample. The chitosan content and thermal properties of Na^+MMT:CS nanocomposite were measured by thermogravimetric analysis (TA Series and TGA Mettler). TGA was performed under a nitrogen gas flow from 20 ºC to 900 ºC at a heating rate of 10 ºC/min.

XRD characterization has been carried out using a Panalytical X'Pert PRO (Cu K_α radiation) diffractometer, with a PIXcel detector, a solid-state detector with rapid readout time and high dynamic range. Data collection has been performed between 5° and 80° 2θ, with a step of 0.02° 2θ.

The surface morphology and microstructure of the nanocomposites were evaluated with scanning electron microscopy (SUPRA™ 40 (ZEISS)). Mucoadhesion studies were done with scanning electron microscopy (FE-SEM Σigma, Lamarx). Samples for X-ray fluorescence analysis were tablets of the pure components and the complexes and it was analyzed on a Rigaku ZSX XRF spectrometer.

2.5 In vitro drug release studies

In vitro drug release behavior of CLX from the pure drug and the nanocomposite carriers were conducted at room temperature with the dialysis bag technique (Joshi, 2009). The CLX release experiments were carried out at pH 1.2 (0.1 M HCl) and at pH values of 4.2 and 6.8, prepared by mixing acetic acid: sodium acetate (55:45). The dialysis bags (Mw cut off 12,000-14,000 Da) were equilibrated with the release medium for few hours prior to release studies. The weighed quantities of beads (containing 50 mg of CLX) were placed in dialysis bags containing 5 ml of the release medium. The dialysis bags were placed into the receptor compartment containing 200 ml of the release medium, which was stirred at 500 rpm at 25 ± 0.5 ºC. A 5 ml aliquot was withdrawn at regular time intervals and the same volume was replaced with a fresh release medium. Samples were analyzed for drug content by UV spectrophotometer at λ_{max} = 255 nm. These studies were performed in triplicate for each sample and the average values were used in data analysis. The release amount of CLX was expressed as percentage of the drug in the release medium respect to the initial amount of CLX in the bag.

2.6 Drug release kinetics

The drug release kinetics was investigated, and data were fitted using the model of Korsmeyer-Peppas (Korsmeyer et al., 1983).

To this purpose initial 60% release values were fitted to the Korsmeyer-Peppas equation (Korsmeyer et al., 1983) as follows,

$$\frac{M_t}{M_\alpha} = Kt^n \qquad (1)$$

which in logarithmic form is:

$$\log \frac{M_t}{M_\alpha} = \log K + n \log t \qquad (2)$$

where M_t/M_∞ is the fraction of drug release from the nanocomposite formulations at time t, K is the rate constant, n is the diffusion exponent and t is the release time.

Values of n between 0.5 and 1.0 indicate anomalous transport kinetics (non-Fickian) and n value of approximately 0.5 indicates the pure diffusion controlled mechanism (Fickian

diffusion). The smaller values of $n < 0.5$ may be due to drug diffusion partially through a swollen matrix and water filled pores in the formulations (Korsmeyer et al., 1983).

2.7 Scanning Electron Microscopy (SEM) for investigating mucin nanocomposite carriers interactions

Mucins were rehydrated in PBS buffer pH 7.4 at a concentration of 0.1 mg/ml (which produced a material with elastic dominant gel like properties) with and without the nanocomposite formulations at 1 mg/ml as above. After 18 h equilibration at room temperature, drops of the resultant mucin gels were dried by vacuum and subsequently sputtered with gold before imaging in the scanning electron microscope. Imaging was done using an accelerating voltage of 3 kV and the secondary electron detector on an electronic microscope.

2.8 In vitro antibacterial activity

Antibacterial activity was evaluated *in vitro* by the disk diffusion test against a reference strain of *Staphylococcus aureus* ATCC 25923 and clinical strains of *Staphylococcus aureus*: 235, 787, 2127, 2804, 2387, 123, 43300.

Mueller-Hinton milieu was used throughout the test. Molten Mueller-Hinton agar with a volume of 15 ml was poured into sterile disposable Petri dished (ϕ: 90 mm). Cultures were prepared in 10 ml of sterile Mueller-Hinton broth and were incubated for 18 h. Cultures were vortexed and a 1/10 dilution in PBS was prepared. This 1/10 dilution was spread on the surface of Petri plates. Paper disks (ϕ: 8 mm) impregnated with CLX (control) and Na^+MMT:CS, CLX/Na^+MMT and CLX/Na^+MMT:CS bionanocomposites were placed in these Petri plates. The experiments were performed in triplicate. After incubation at 37 ºC for 24 h, the inhibition zone was measured from one edge of the zone of inhibition to the opposite edge, including the diameter of the disk. The diameters of the inhibition zones in agar plates are given in mm.

3. Results and discussion

3.1 *Characterization*

To know whether added CS enters into the interlayer of the clay mineral or not, XRD analyses were done to measure d-spacing of sodium montmorillonite (Na^+MMT). This value represents the thickness of the clay platelet plus the interlayer distance (Pasparakis & Bouropoulos, 2006 and Bertagnolli et al., 2011). Fig. 1 shows XRD patterns of nanocomposites and their pure components.

The diffractogram of the Na+MMT sample without CS (Fig .1Aa) presented a basal spacing peak at 2θ ~ 9°, indicating that the thickness of the Na+MMT silicate layer was 12.5 Å. CS showed typical pattern of a low crystalline powder, with diffraction bands around 2θ ~ 10º, 20º and 40º. These low intensity reflections are due to the crystalline regions formed by hydrogen bonds among the amino and hydroxyl groups on chitosan chains (Fig.1Ac) (Eloussaief et al., 2011).

For the Na^+MMT:CS nanocomposite (Fig. 1Bb), the basal diffraction at about 12.5 Å of the clay is slightly shifted to an higher angle, that is a smaller d-spacing. Thus, the observed decrease in the basal spacing indicates that Na^+MMT keeps the original crystal structure and exists as primary particles in the CS matrix, since the observed increase in the basal spacing can be considered as quite limited. Probably, due to the coiled structure of CS, its intercalation only occurs in the planar conformation, so that, although polymer molecules were effectively trapped inside the clay interlayer, part of them could remain at the outer surface of the clay particles. The results are in good agreement with those obtained by other authors (Celis et al., 2012 and Günister et al., 2007). The XRD patterns of CLX/Na^+MMT and CLX/Na^+MMT:CS nanocomposites are shown in Figs. 1Bc and 1Bd, respectively. Interactions of Na^+MMT with CLX did not increase the d-spacing of the Na^+MMT, yielding a diffraction pattern less resolved as compared with the diffraction pattern of the pure Na^+MMT, probably as a result of interactions between CLX and the Na^+MMT surface (Fig.1Bc). This result indicated that CLX was mostly adsorbed on the surface of Na^+MMT, however, a partial intercalation of CLX between the Na^+MMT layers cannot be excluded. Similar result was observed with the

CLX/Na^+MMT:CS nanocomposite (Fig.1Bd), exhibiting its diffraction pattern little difference in basal spacing of Na^+MMT and broad peaks, indicating that CS was mainly adsorbed on the surface or led to the very less intercalation to Na^+MMT.

The chemical composition of Na^+MMT, MMT, Na^+MMT:CS and MMT:CS powders was measured by XRF (Table 1). The results clearly indicate the presence of sodium, aluminum and silicon in Na^+MMT, and of carbon but no sodium in the MMT:CS nanocomposite. The carbon content (15% mass) in the nanocomposite indicates the presence of organic matter in the resulting Na^+MMT:CS nanocomposite system, since the CS was the only source of this element. In addition, the disappearance of sodium content in Na^+MMT:CS could result from the exchange of sodium ions by CS cations after interaction of the polymer.

FTIR spectra of nanocomposites and their pure components were compared to examine the possible interactions mechanisms (Fig. 2). The clay mineral FTIR spectrum (Fig. 2a) showed a broad and composite absorption between 3444 cm^{-1} and 3621 cm^{-1} due to hydroxyls of the clay matrix and of the adsorbed water, and an intense absorption in the range 1000-1200 cm^{-1} due to Si-O-Si stretching of the silicate. Also, the characteristic band at 1632 cm^{-1} ascribed to the water molecules (physisorbed, H-bonded and directly coordinated to the exchangeable cations of the clay) was observed in the Na^+MMT spectrum (OH bending of adsorbed water) (Hua et al., 2010 and Aguzzi et al., 2014). The CS spectrum (Fig. 2b) exhibited the peak associated to the vibration of carbonyl bonds of amide groups CONH-R at 1656 cm^{-1} and the peak at 1587 cm^{-1} corresponding to the vibrations of amine group (NH_2) (Fong et al., 2010). Also, the FTIR spectrum of CS showed a broad band between 3100 cm^{-1} and 3700 cm^{-1} due to –OH groups and –NH groups.

The FTIR spectrum of CLX (Fig. 2c) showed the characteristic bands of this drug, that are that at 1640 cm^{-1} corresponding to the double bond C=N-H strectching vibration (Paluszkiexicz et al., 2011), as well as those corresponding to the aromatic C=C stretching modes located at about 1520 cm^{-1} and 1400 cm^{-1} The peaks at 2923 and 2864 cm^{-1} were attributed to the CH_2C-H stretching of methylene groups of CLX (Musial, 2011).

The peak at 1587 cm^{-1} of the $–NH_2$ group in the starting CS was not observed in the Na^+MMT:CS nanocomposite spectrum (Fig.2d), whereas a band appeared at 1514 cm^{-1}

corresponding to the deformation vibration of the protonated amine group (-NH_3^+) of chitosan was displayed, indicating an electrostatic interaction between the cationic polymer and the negatively charged clay groups (Chen et al., 2008). This result was in agreement with the results from XRD and XRF, revealing the intercalation of CS in the MMT structure.

In the case of the CLX/Na^+MMT nanocomposite (Fig. 2e), new bands in the 3400-3200 cm^{-1} region are due to the asymmetric and symmetric NH stretching modes of CLX were observed (Dader et al., 2003). The band at about 1640 cm^{-1} is ascribed to the C=N band of the pure CLX superimposed to the bending mode of interlayer water.

Fig. 2f shows the FTIR spectrum of the CLX/Na^+MMT:CS ternary nanocomposite. It was observed a band at about 3627 cm^{-1} due to –OH stretching mode of Al-OH, the band in the range 1000-1200 cm^{-1} due to Si-O-Si stretching of the silicate. Bands in the range 3500-3300 cm^{-1} are due the asymmetric and symmetric NH stretching vibrations of both CLX and CS, the peaks at 2926 cm^{-1} and 2862 cm^{-1}, attributed to the CH_2C-H stretching of methylene groups of CLX. The ν(C=N) stretching vibration of the imine group of CLX appears at 1632 cm^{-1}, probably overlapped to the bending mode of adsorbed water. Modes of CLX aromatic rings appear in the range 1550-1300 cm^{-1}. The overlapping of CLX bands with those of CS and Na^+MMT prevents a clear description of the interactions among the three components in the system.

Fig.3 displays TGA and DTG curves obtained for CS, Na^+MMT, the CS:Na^+MMT nanocomposite and the CLX nanocomposites (CLX/Na^+MMT and CLX/Na^+MMT:CS). TGA and DTG curves corresponding to the CS (Fig.3a) showed three thermic process at 81º, 294º and 503 ºC, respectively. The first one, associated with a weight loss of 8.6%, was attributed to the loss of physically adsorbed water molecules. The others one at 294 ºC (weight loss of 59%) and 504 ºC (weight loss of 33%) were related to the pyrolytic decomposition followed by the combustion of the biopolymer (Holesova et al., 2014 and Zohuriaan & Shokrolahi, 2004). With regard to pure Na^+MMT (Fig. 3b), the initial loss (between 25 and 150 ºC) is related to dehydratation of adsorbed water (non-constitutional water), interlayer water, and water coordinated to exchangeable cations (structural water). The mass loss above 350 ºC corresponds to elimination of structural hydroxyl (Waymack et al., 2004). The absence of a defined peak in the DTG curve of Na^+MMT indicated that dehydroxylation occurred gradually and at a uniform rate.

TGA/DTG curves of the Na^+MMT:CS nanocomposite (Fig. 3c) displayed peaks at 92º and 248 ºC. The modification of Na^+MMT with the organic polymer increased the number of descomposition steps. The first step corresponds to the onset of decomposition of organic matter around 200 ºC, with the maximum decomposition occurring around 248 ºC. The second step is mainly attributed to the chemical decomposition of the bonded structure of the organic polymer around 400 ºC. The DTG peaks corresponding to CS decomposition have been shifted toward lower temperature values, appearing at 248 ºC, being associated with a weight loss of 10.4%. The water content of this nanocomposite was 2% at 92 ºC, due to the hydrophilic character of both components, CS and Na^+MMT. The content of CS in the Na^+MMT:CS powder calculated from weight loss of the TGA thermograms was about 14 mass%. These findings fit with results obtained from XRF.

On the other hand, the TGA/DTG curves of the Na^+MMT/CLX nanocomposite (Fig. 3d) displays several peaks around 76º, 183.5º, 326º and 480.5 ºC, respectively and a shoulder at 217 ºC. As indicated by the TGA and DTG curves of Na^+MMT (Fig. 3b), montmorillonite is thermally stable in the temperature range of 200-500 ºC, hence, the weight loss in this temperature range should be attributed to the evaporation and/or decomposition of CLX adsorbed, or possibly also partially intercalated into the organoclay space due to it was difficult to determine, from the XRD studies, whether CLX has been intercalated into the interlayer space of Na^+MMT because of its unchanged basal spacing. The shoulder at 217 ºC corresponds to the evaporation of physically adsorbed CLX, while peaks at 326º and 480.5 ºC were assigned to the oxidation of residual CLX (Holešová et al., 2014).

The total weight loss of the CLX/Na^+MMT:CS composite was ~20% (Fig 3e). The DTG curve showed the absence of a defined peak, indicating that the CS and CLX degradation in the nanocomposite occurred gradually and at uniform rate. This result suggested higher thermal stability of the organic matter when intercalated into the clay mineral.

The morphologies and microstructure of the samples were characterized by SEM (Fig. 4). Fig. 4a shows that the Na^+MMT displays a layered structure with platelet morphology consisting of stacked siliciate sheets. In the SEM images of the Na^+MMT:CS systems (Fig. 4 b) stacked flakes (stacks of multilayers of Na^+MMT) and flocculated fraction of Na^+MMT was observed,

which might be consistent with CS adsorbed on the Na^+MMT surface and/or irregular intercalation of Na^+MMT by CS (He et al., 2006).

3.2 In vitro drug release experiments

Because the pH value of saliva ranges between 6.0 and 7.5 (Aframian et al., 2006), however, during infection the environment tends to become acidic due to combined actions of bacterial metabolism and the host immune response (Radovic-Moreno et al., 2012), the release responses of the pure CLX and CLX nanocomposites carriers with Na^+MMT, with or without CS, were studied at three different pH values (1.2, 4.2 and 6.8) to mimic the pathophysiological conditions of the oral cavity and exploiting the CLX nanocomposites usage as pH-responsive drug delivery systems for treating bacterial infections." On the other hand, sublingual temperature is routinely used as an indicator of oral temperature and when measured under specific conditions it approximates 37 ºC for most individuals. It cannot, however, be assumed that this represents the true resting temperature for all sites within the oral cavity (Barclay et al., 2005; Aframian et al.; 2006, Choi et al., 2015). Since, the oral cavity undergoes frequent and drastic fluctuations in temperature, we found no differences in the release profiles of the studied systems at 25 ºC or 37 ºC (data don not shown), and we had better control of the temperature of the experiments at 25 ºC, we decided to choose this temperature for performing the release studies.

Concerning the release profiles of CLX systems (Fig 5), it was found that the release of the pure CLX was very rapid at pH values of 4.2 and 6.8. In contrast, drug release was less rapid at the pH value of 1.2. However, there was an initial burst release of CLX in all the investigated pH values.

The release of the drug after 24 h from the clay matrix at pH 1.2, 4.2 and 6.8 was ~20%, ~10% and ~5%, respectively, while the CLX release after 24 h from the Na^+MMT:CS composite at pH 1.2, 4.2 and 6.8 was ~35%, ~30% and ~20%, respectively (Table 2). Thus, the percentage cumulative drug release followed the sequence CLX > CLX/Na^+MMT:CS > CLX/Na^+MMT at the examined pH values.

It may be noted from Fig. 5 that the drug release rate from the clay and clay-chitosan nanocomposite particle carriers was constant. There was no initial burst release found in both

formulations. The more controlled release profiles of CLX from the nanocomposite systems compared to the pure CLX offer the possibility of drug release carriers for applications where relatively slower profiles are desirable. For passive delivery to the oral cavity the drug delivery system should be capable of retaining the drug for a prolonged period of time, thus, facilitating a controlled and sustained release of the drug without any initial burst release.

In clay and clay-chitosan nanocomposite particle carriers the positively charged CLX bound strongly to the negatively charged clay and the release of CLX is very slow.

The negative charge on clay increases with increasing pH, while drug (pK_{a1}~2.2; pK_{a2} ~10.3) remains positively charged even at pH 6.8. This indicates that drug binds even more strongly to clay, and therefore it is slowly release from the clay after 24 h at pH 6.8. The presence of the biopolymer in the composite influences the interaction between drug and clay, which in turn accelerated the release of the drug from drug-biopolymer/clay composite. Thus, drug release was comparatively faster from the composite than from the pure clay at the three pH values. Moreover, the presence of biopolymer in the composite is reported to result in mucoadhesion and promote bioavailability of the drug by interacting with the oral mucosa. Thus, the release of drug from the composite could be tuned by controlling the amount of biopolymer in the composite. Thus, a significant finding was that the cumulative CLX release from the chitosan-clay nanocomposite particle carrier was intermediate between the pure CLX and the clay, i.e lower than pure clay and significantly greater than CLX/Na^+MMT nanocomposite, at all three investigated pH values.

3.3 Drug release kinetics

"Data obtained from *in vitro* drug release of each nanocomposites were fitted into four different kinetic models: zero order, first order, Higuchi and Kormeyer-Peppas models (Singhvi and Singh, 2011), however, it was obtained better fit and high values for r^2 with the Kormeyer-Peppas model, suggesting that this model seems to be more suited and hence was subsequently used to describe release kinetics of the studied systems."

The values of correlation coefficient (r^2), n value and rate constants (k) for Korsmeyer-Peppas kinetic model are presented (Table 2). Taking into account the values of "n", drug release

from drug/clay mineral and drug-clay/biopolymer composites followed drug diffusion partially through a swollen matrix and water filled pores in the formulations.

3.4 Porcine gastric mucin studies

Adhesive interactions between porcine gastric mucin (PGM) and CLX nanocomposite carriers were conducted to establish the mucobioadhesive properties of the CLX formulations. The PGM has structural and functional properties similar to mucins of other origins (Oh et al., 2015), and thus it was used as a model of the oral mucin. Scanning electron microscopy (SEM) was utilized to detect structural changes that occurred upon the addition of the CLX nanocomposite carriers.

The main difference between our study and others one reported, is that we examined the structure of hydrated mucin, which allowed us to observe the actual structural array of mucin fibers, since gastric mucus is a highly hydrated (swollen to ~95% water), since biological samples for SEM considers fixation, dehydratation and drying, and such procedures strongly stress the delicate filamentous structure of glycoprotein matrices.[41] Therefore, we did not use fixation and dehydration procedures to prepare the SEM samples.

Fig. 6a shows the SEM image of a mucin layer gel. Reveals a swollen network formed by the glycoprotein mucin. Mucin is in a hydrated state, so the fibers are expanded and occupy the entire volume of the mucin gel.

Mucus is an entangled fiber matrix with many weak non-covalent interactions such as hydrogen bonding and electrostatic interactions. Mucins are glycoproteins of the mucus gel present on mucosal surfaces. Mucins form a fully hydrated viscoelastic gel layer known as mucus. Almost all mucins are negatively charged due to the presence of anionic sialic, sulfate and carboxyl functional groups (Ashton et al., 2013 and Barz et al., 2012). It is a negatively charged hydrogel with the matrix tangled in a randomly woven polyionic network.

Microstructural images of PGM with added the CLX/Na^+MMT are showed in Fig. 6b. It was observed that PGM adsorbed on the negatively charged Na^+MMT surface arranged in dispersed globules of aggregated mucin molecules. These compact spherical structures of mucin are

compatible with the aggregation of several mucin molecules. At physiological pH, mucin is negatively charged due to the sialic acid residues on the carbohydrate-rich regions of the molecules (Willits et al., 2001). Therefore, interactions between Na^+MMT negative surface and mucin should be limited by electrostatic repulsion.

Microstructural images of PGM with added the CLX/Na^+MMT:CS system are shown in Fig. 6c. The addition of the CLX/Na^+MMT:CS nanocomposite caused a noticeable change in the mucin network. In this case, mucin is arranged in compact fiber-like structures. The fibers appear to aggregate together, leaving holes in the fiber network adjacent to regions with very small interfiber spacing. The fiber aggregation is likely due to the electrostatic interactions between the chitosan and the mucin. In fact, the glycans of mucins are mainly terminated with sialic acid and sulfate groups, which can electrostatically interact with positively charged nanoparticles (e.g., chitosan). It is known that CS possesses mucoadhesive properties, due to the presence of many amino groups in the polymer chains that form hydrogen bonds with glycoproteins in the mucus and also ionic interactions between positively charged amino groups and negatively charged sialic acid residues of mucin (Silva et al., 2012 and Albarkah et al., 2015).

Although the conditions used in this model system are simpler than the typical *in vivo* environment, the resulting knowledge will enable the rational design of CS-based nanostructured materials for specific transmucosal drug delivery.

Mucoadhesion has a significant role in drug delivery via mucosal routes of administration by retaining the formulation at the site of administration, thereby, improving the drug absorption and drug bioavailability. Furthermore, mucoadhesive materials can be used as curative agents to cover and protect damaged tissues (such as gastric ulcers or lesion of oral mucosa) or work as coating agents.

3.5 In vitro antibacterial activity

Disk diffusion test results of CLX (control), Na^+MMT:CS, CLX/Na^+MMT and CLX/Na^+MMT:CS nanocomposites are shown in Fig. 7. The Na^+MMT:CS nanocomposite showed no inhibitory zone for all strains of *S. aureus*, reflecting no antibacterial activity.

However, CLX, CLX/Na^+MMT and CLX/Na^+MMT:CS systems showed a very clear inhibition zone around the specimen. The results from the zone of inhibition tests are given in Table 3. The presence of zone of inhibition is an indication of the diffusion of the antibacterial drug CLX from the Na^+MMT and the Na^+MMT:CS nanocomposites into the agar media, maintaining the CLX antimicrobial properties .

4. Conclusions

The incorporation of CS into Na^+MMT by ion exchange mechanism took place, probably partially within the interlayer space and on the surface of the mineral clay. The resulting Na^+MMT:CS hybrids were further compounded with CLX and CLX/Na^+MMT:CS nanocomposite beads were successfully prepared

The *in vitro* drug release test results clearly suggested that Na^+MMT for the hybrid material, and Na^+MMT along with CS for the composite beads were able to control the release of CLX, by making it sustained, without any burst effect, and by reducing the release amount and the release rate. Moreover, they do not quench the antimicrobial properties of the drug.

The CLX loaded Na^+MMT:CS nanocomposite carrier exhibited good mucoadhesive properties. This characteristic enables the drug delivery system to stay longer at the absorption site, and therefore, it could give a beneficial effect on the drug bioavailability.

In conclusion, the CLX/Na+MMT:CS composite beads may be a promising candidates for the treatment of buccal infections.

Acknowledgment

The authors thank FONCyT (Préstamo BID 1728/OC-AR, PICT 1376), the Secretaría de Ciencia y Técnica de la Universidad Nacional de Córdoba (SECyT), the Consejo Nacional de Investigaciones Científicas y Tecnológicas de la Nación (CONICET) for their financial support and Euro Tango 2 project, supported by European Commission and EACEA, Erasmus Mundus Action 2-strand 1. The authors also thank to Dra Silvia Ronchetti for analyzing XRD data.

References

Aduba, D. C., Hammer, J. A. Jr., Yuan, Q., Yeudall, W. A., Bowlin, G. L., Yang., H. 2013. Semi-interpenetrating network (sIPN) gelatin nanofiber scaffolds for oral mucosal drug Delivery. Acta Biomater. , 9, 6576–6584.

Aframian, D.J., Davidowitz, T., Benoliel R. 2006. The distribution of oral mucosal pH values in healthy saliva secretors. Oral Dis., 12(4), 420-423.

Aguzzi, C., Cerezo, P., Viseras, C., Caramella, C. 2007. Use of clays as drug delivery systems: Possibilities and limitations. Appl. Clay Sci., 36, 22-36.

Aguzzi, C., Sandri, G., Bonferoni, C., Cerezo, P., Rossi, S., Ferrari, F., Caramella, C., Viseras, C. 2014. Solid state characterisation of silver sulfadiazine loaded on montmorillonite/chitosan nanocomposite for wound healing. Colloids Surf. B Biointerfaces, 113, 152-157.

Albarkah, Y.A., Green, R.J., Khutoryanskiy, V.V. 2015. Probing the mucoadhesive interations between porcine gastric mucin and some water-soluble polymers. Macromolec. Biosci., 15, 1546-1553.

Ariga, K., Ji, Q., McShane, M.J., Lvov, Y.M., Vinu, A., Hill, J.P.2012. Inorganic nanoarchitectonics for biological applications. Chem. Mater., 24, 728-737.

Ashton, L., Pudney, P.D.A., Blanch, E.W., Yakubov, G.E. 2013. Understanding glycoprotein behaviours using Raman and Raman optical activity spectroscopies: characterizing the entanglement induced conformational changes in oligosaccharide chains of mucin. Adv. Colloid Interface Sci., 66-77.

Barclay, C.W., Spence, D., Laird, W.R.E. 2005. Intra-oral temperatures during function. J. Oral Rehabil., 32, 886-894.

Barz, B., Turner, B.S., Bansil, R., Urbane, B. 2012. Folding of pig gastric mucin non-glycosylated domains: a discrete molecular dynamics study. J. Biol. Phys., 681-703.

Bertagnolli, C., Kleinübing, S.J., da Silva, M.G.C. 2011. Preparation and characterization of a Brazilian bentonite clay for removal of copper in porous beds. Appl. Clay Sci., 53, 73–79.

Besinis, A., De Peralta, T., Tredwin, C.J., Handy, R.D. 2015. Review of nanomaterials in dentistry: interactions with the oral microenvironment, clinciasl applications, hazards, and benefits. ACS Nano, 9, 2255-2289.

Celis, R., Adelino, M.A., Hermosín, M.C., Cornejo, J. 2012. Montmorillonite-chitosan bionanocomposites as adsorbents of the herbicide clopyralid in aqueous solution and soil/water suspensions. J. Hazard. Materials, 67-76.

Choi, J.E., Loke, C., Waddell, J.N.., Lyons, K.M., Kieser, J.A., Farella, M. 2015. Continuous measurement of intra-oral pH and temperature: development, validation of an appliance and a pilot study. J. Oral Rehabil. 42, 563-570.

He, H., Frost, R.L., Yuan, P., Duong, L., Yang, D., Xi, Y., Kloprogge, J.T. 2006. Changes in the morphology of organoclays with $HDTMA^+$ surfactant loading. Appl. Clay Sci., 31, 262-271.

Hen, C. L., Bromberg, L., Atton, H.T.A., Rutledge, G.C. 2008. Electrospun cellulose acetate fibers containing chlorhexidine as a bactericide. Polymer 49, 1266–1275.

Chiu, C-W., Lin, J.-J. 2012. Self-assembly behavior of polymer-assisted clays. Progr. Polym. Sci., 37, 406-444.

Darder, M., Colilla, M., Ruiz-Hitzky, E. 2003. Biopolymer-clay nanocomposites based on chitosan intercalated in montmorillonite. Chem. Mater., 15, 3774-3780.

dos Santos Miranda Costa, I., Pereira Abranches, R., Junqueira García, M.T., Riemma Pierre, M.B. 2014. Chitosan-based mucoadhesive films containing 5-aminolevulinic acid for buccal cancer´s treatment. J. Photochem. Photobiol. B: Biology 140, 266-275.

Eloussaief, M., Kallel, N., Yaacoubi, A., Benzina, M. 2011. Mineralogical identification, spectroscopic characterization, and potential environmental use of natural clay materials on chromate removal from aqueous solutions. Chem. Engineering Journal, 168, 1024–1031.

Familiari, G., Relucenti, A., Amiliari, F A., Battaglione, E., Franchitto, G., Heyn, R. 2007. Visualization of the real microarchitecture of glycoprotein matrices with scanning electron microscopy. Modern Res. Educal. Topics Microsc., 224-228.

Fengwei Xie, D., Martino, V.P., Sangwan, P., Way, C., Cash, G.A., Pollet, E., Dean, K.M., Halley, P.J., Aérous L. 2013. Elaboration and properties of plasticized chitosan-based exfoliated nanobiocomposites. Polymer, 54, 3654-3662.

Fong, N., Simmons, A., Poole-Warren L.A. 2010. Antibacterial polyurethane nanocomposites using chlorhexidine diacetate as an organic modifier. Acta Biomater. 6, 2554-2561.

Günister, E., Pestreli, D., Ünlü, C.H N., Güngör, N. 2007. Synthesis and characterization of chitosan-MMT biocomposite. Carb. Polym. 67, 358-365.

Holesova, S., Stembirek, J., Bartosova, L., Prazanova, G., Valaskova, M., Samlikova, M., Pazdziora, M. 2014. Antibacterial efficiency of vermiculite/chlorhexidine nanocomposites and results of the in vivo test of harmlessness of vermiculite. Mater. Sci. Eng. C, 42, 466-473.

Hua, S., Yang, H., Wang, W., Wang, A.. 2010. Controlled release of ofloxacin from chitosan-montmorilloniet hydrogel. Appl. Clay Sci., 50, 112-117.

Kaemkit, C., Monvisade, P., Siriphannon, P., Ukeaw, N J. 2013. Water-soluble chitosan intercalated montmorillonite nanocomposites for removal of basic blue 66 and basic yellow 1 from aqueous solution. J. Appl. Polym. Sci., 128, 879-887.

Kolahi, J., Soolari, A. 2006. Rising with chlorhexidine gluconate solution after brushing and flossing teeth: A systematic review of effectiveness. Quintessence Intern., 37, 605-612.

Korsmeyer, R.W., Gurny, R., Doelker, E., Buri, P., Peppas, N.A.. 1983. Mechanisms of solute release from porous hydrophilic polymers. Inter. J. Pharm., 15, 25-35.

Koukaras, E.N., Papadimitriou, S.A., Bikiaris, D.N., Froudakis, G.E. 2012. Insight on the formation of chitosan nanoparticles through ionotropic gelation with tripolyphosphate. Mol. Pharm., 9, 2856-2862.

Li, B., Robinson, J.R. Preclinical assessment of oral mucosal drug delivery systems, in: T.K.Ghosh, W.R. Pfister (Eds.), Drug Delivery to the Oral Cavity: Molecules to Market, CRC Press, Boca Raton, FL, 2005, pp. 41–66.

Marroquin, J.B., Rhee, K.Y., Park, S.J. 2013. Chitosan nanocomposite films: enhanced electrical conductivity, thermal stability, and mechanical properties. Carb. Polym., 92, 1783-1791.

Musial, W. 2011. The deposition of chlorhexidine on chemically modified thermosensitive polyNIPA microgels assessed by EDXS in scanning electron microscopy. Latin Am. J. Pharm., 30, 1481–1486.

Oh, S., Wilcox, M., Pearson, P., Borrós, S.. 2015. Optimal design for studing mucoadhesive polymers interaction with gastric mucin using a quartz crystal microbalance with dissipation (QCM-D): comparison of two different mucin origins. Eur. J. Pharm. Biopharm., 96, 477-483.

Paluszkiexicz, C., Stodolak, E., Hasik, M., Blazewics, M. 2011. FT-IR study of montmorillonite-chitosan nanocomposite materials. Spectrochim. Acta Part A: Mol. Biomol. spectrosc., 79, 784-788.

Pasparakis, G., Bouropoulos, N 2006. Swelling studies and in vitro release of verapamil from calcium alginate and calcium alginate-chitosan beads. Int. J. Pharm., 323, 34-42.

Radovic-Moreno, A.F., Lu, T.K., Puscasu, V.A., Yoon, C.J., Langer, R., Farokhzad, O.C. 2012. Surface charge-switching polymeric nanoparticles for bacterial cell wall-targeted delivery of antibiotics. [ACS]NANO, 6(5), 4279-4287.

São Pedro, A., Cabral-Albuquerque, E., Ferreira, D., Sarmento, B. . 2009. Chitosan: An option for development of essential oil delivery systems for oral cavity care?. Carb. Polym., 76,501-508.

Silva, C.A., Nobre, T.M., Pavinatto, F.J, Oliveira,O.N. 2012. Characterization of bonding between poly(dimethylsiloxane) and cyclic olefin copolymer using corona discharge induced grafting polymerization. J. Coll. Interface Sci., 289-295.

Singhvi, S., Singh, M. 2011. Review: in vitro drug release characterization models. IJPSR, II, 77-84.

Sudhakar, Y., Kuotsu, K., Bandyopadhyay, A.K. . 2006. PEG-modified gold nanorods with a stealth character for in vivo applications. J. Control. Rel., 114:15e40.

Viseras, C., Aguzzi, P, Cerezo, C., Bedmar, M.C. 2008. Biopolymer-clay nanocomposites for controlled drug delivery. Mater. Sci. Technol., 24, 1020-1026.

Viseras C., Cerezo, P., Sanchez, R., Salcedo, I., Aguzzi, C. 2010. Current challenges in clay minerals for drug delivery. Appl. Clay Sci., 48, 291-295.

Walsh, T., Oliveira-Neto, J.M., Moore, D. 2015. Chlorhexidine treatment for the prevention of dental caries in children and adolescents. Cochrane Database Syst Rev. 13;4:CD008457. doi: 10.1002/14651858.CD008457.pub2.

Waymack, B. E., Belote, J. L., Baliga, V. L., Hajaligol, M. R. 2004. Effects of metal salts on char oxidation in pectins/uronic acids and other acid derivative. Fuel, 83, 1505-1518.

Willits, R.K., Saltzma W.M. 2001. Synthetic polymers alter the structure of cervical mucus. Biomater., 22, 445-452.

Xu, J., Strandman, S., Hu, Z J.X.X., Barralet, J., Cerruti, M. 2015. Genipin-croslinked catechol-chitosan mucoadhesive hydrogels for buccal drug delivery. Biomater., 37, 395-404.

Zohuriaan, M. J., Shokrolahi, F. 2004. Thermal studies on natural and modified gums. Polym. Test., 23, 575-579.

LEYEND FIGURES

Figure 1. XRD patterns of **A)** sodium montmorillonite, Na^+MMT (a), lyophilized chlorhexidine, CLX (b), chitosan, CS (c); **B)** Na^+MMT (a), Na^+MMT:CS (b), CLX/Na^+MMT (c) and CLX/Na^+MMT:CS (d) nanocomposites.

Figure 2. FT-IR spectra of Na^+MMT (a), CS (b), CLX (c), Na^+MMT:CS (d), CLX/Na^+MMT (e) and CLX/Na^+MMT:CS (f).

Figure 3. TGA (solid line) and DTG (dotted line) of CS (a); Na^+MMT (b) and Na^+MMT:CS (c), CLX/Na^+MMT (d) and CLX/Na^+MMT:CS (e) nanocomposites.

Figure 4. SEM images of sodium montmorillonite, Na^+MMT (a) and Na^+MMT:CS (b) nanocomposites.

Figure 5. Release profiles of CLX formulations at difference pH media.

Figure 6. SEM images of Pig gastric mucin, PGM (a) and PGM with CLX/Na^+MMT (b) and PGM with CLX/Na^+MMT:CS (c).

Figure 7. Photograph of antimicrobial test of CLX (1), CLX/Na^+MMT (2), CLX/Na^+MMT:CS (3) and Na^+MMT:CS (4).

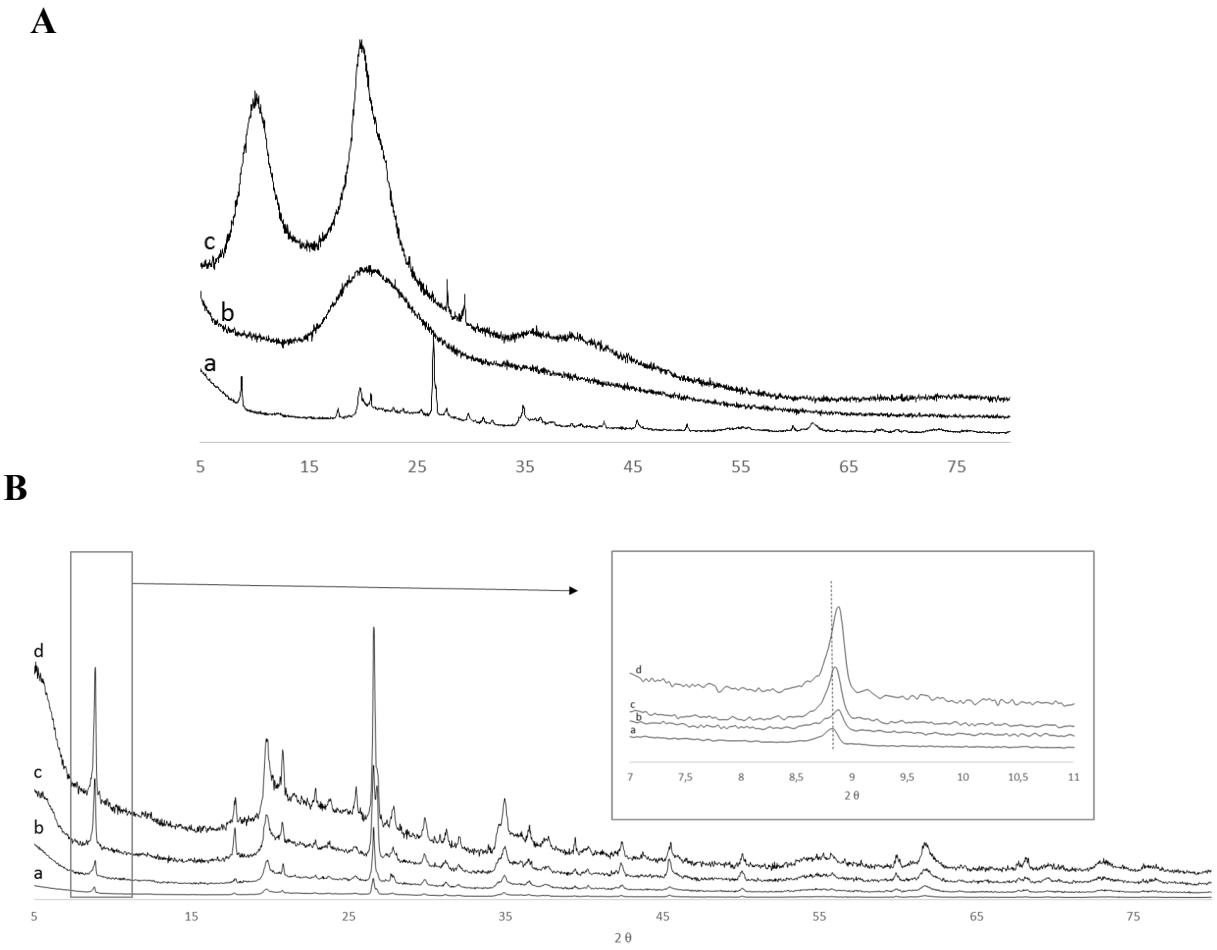

FIGURE 1

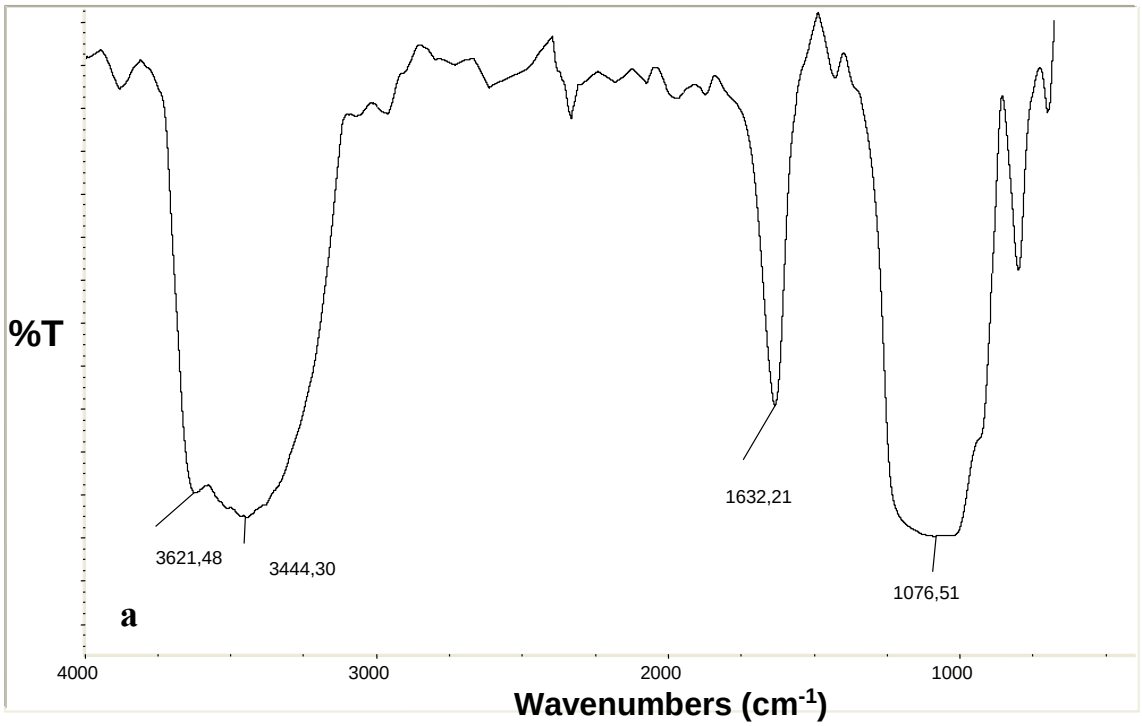

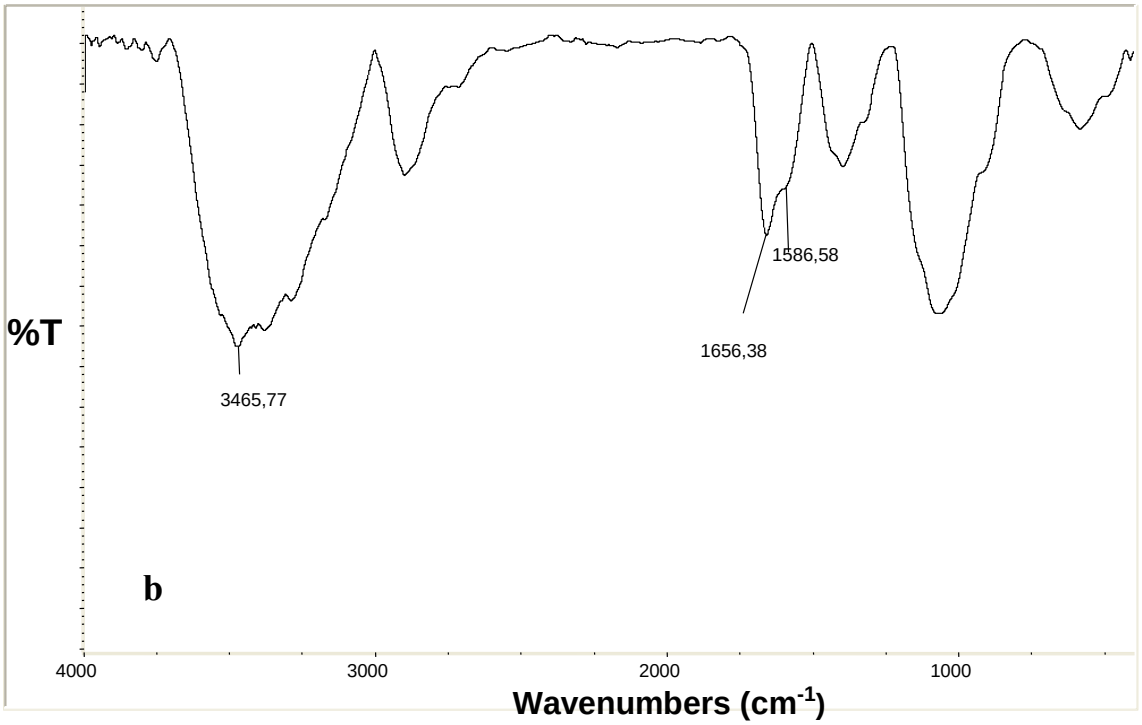

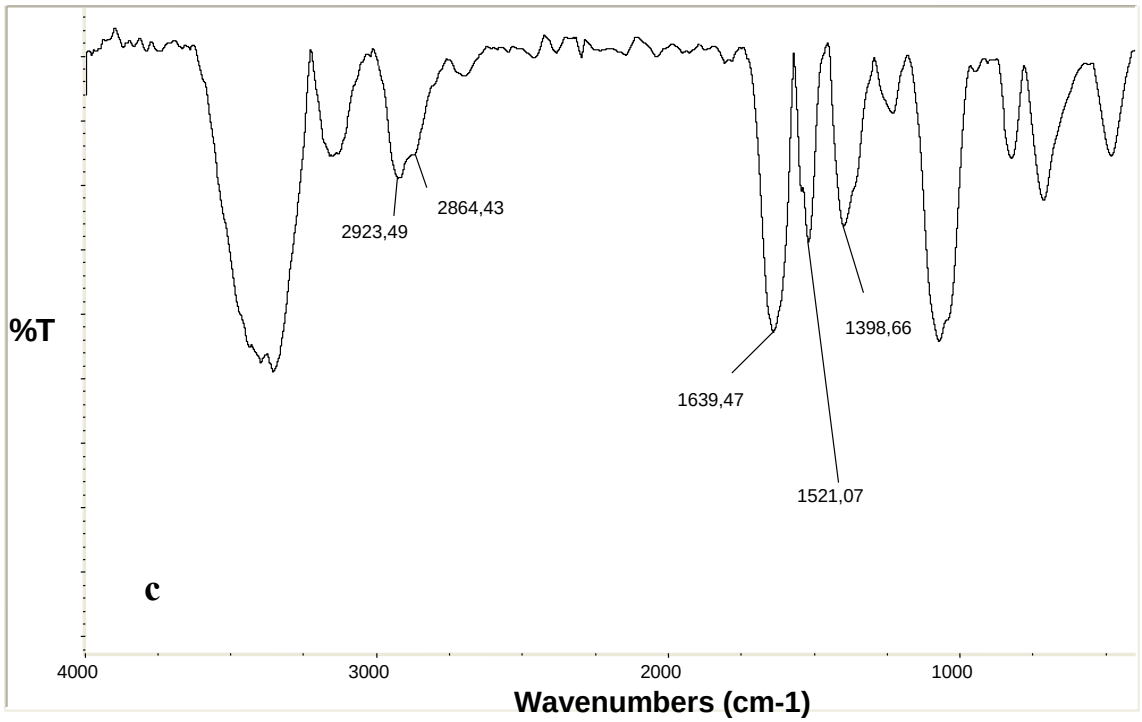

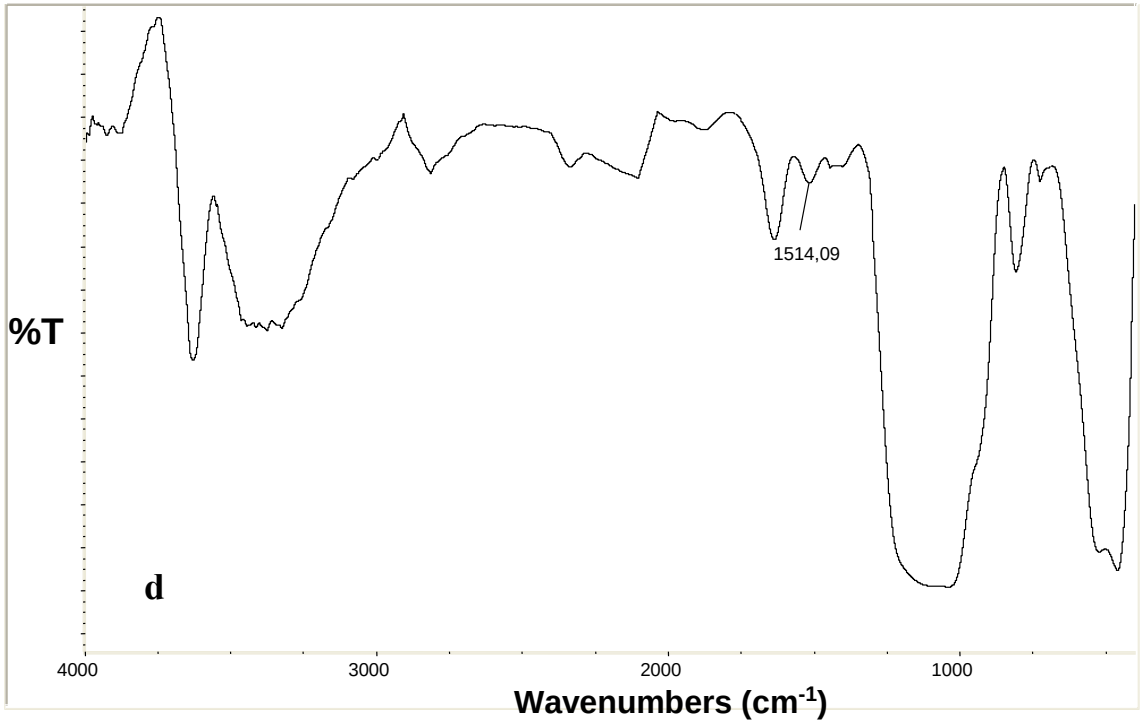

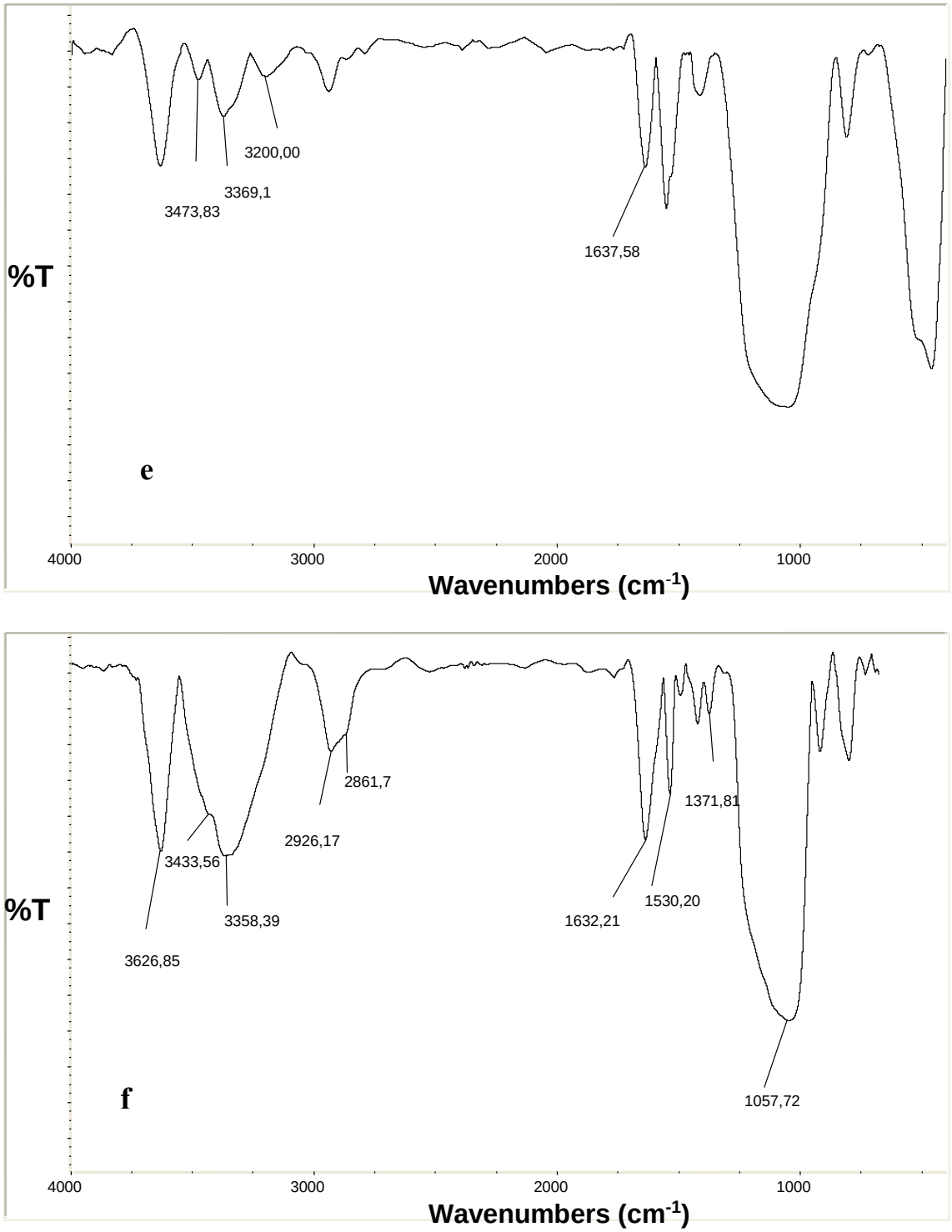

FIGURE 2

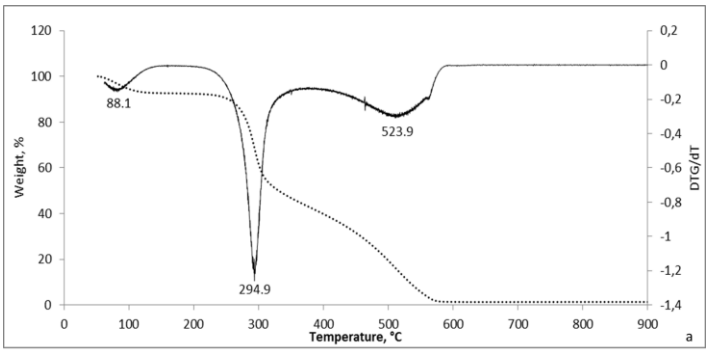

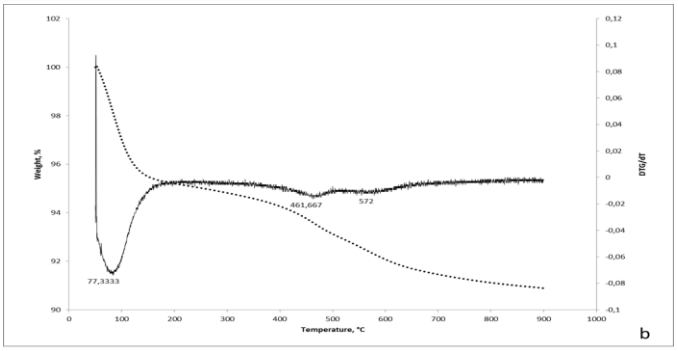

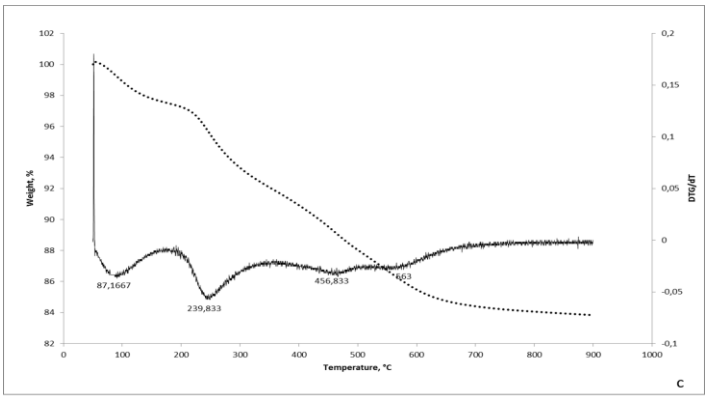

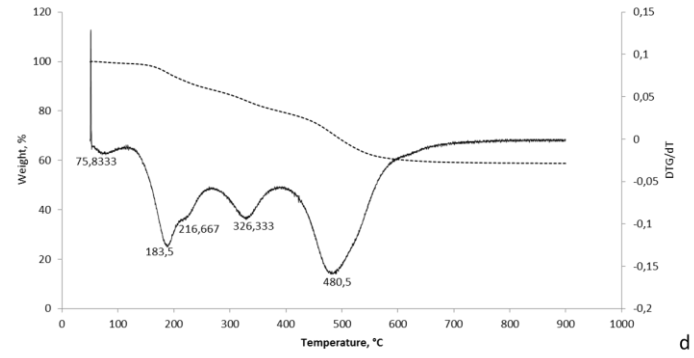

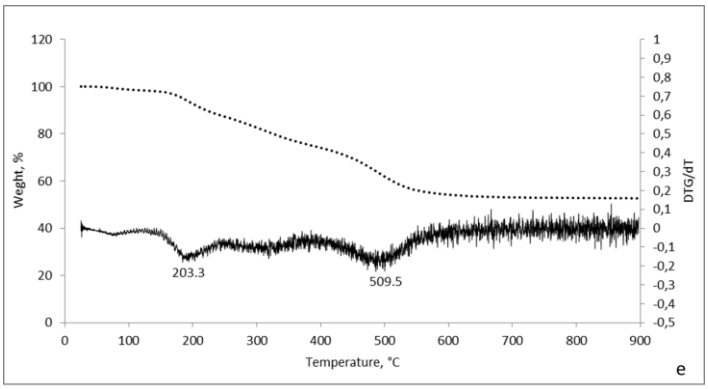

FIGURE 3

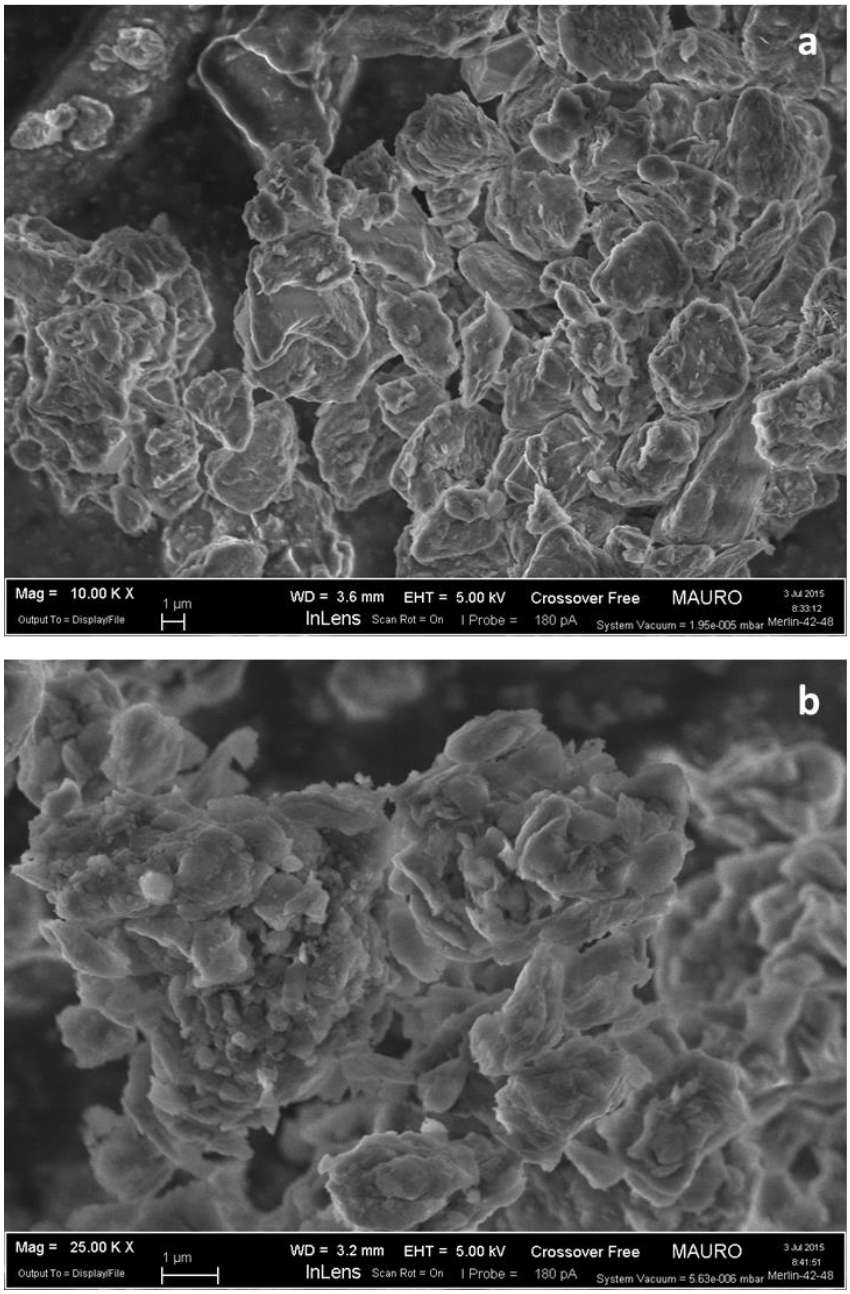

Figure 4

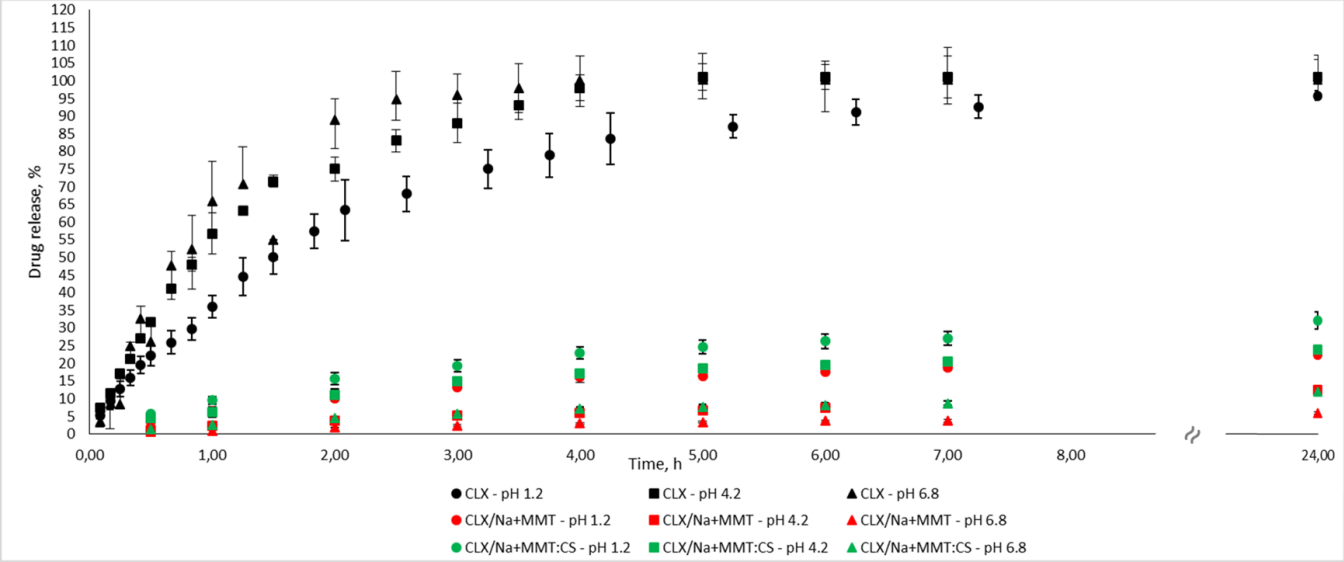

Figure 5

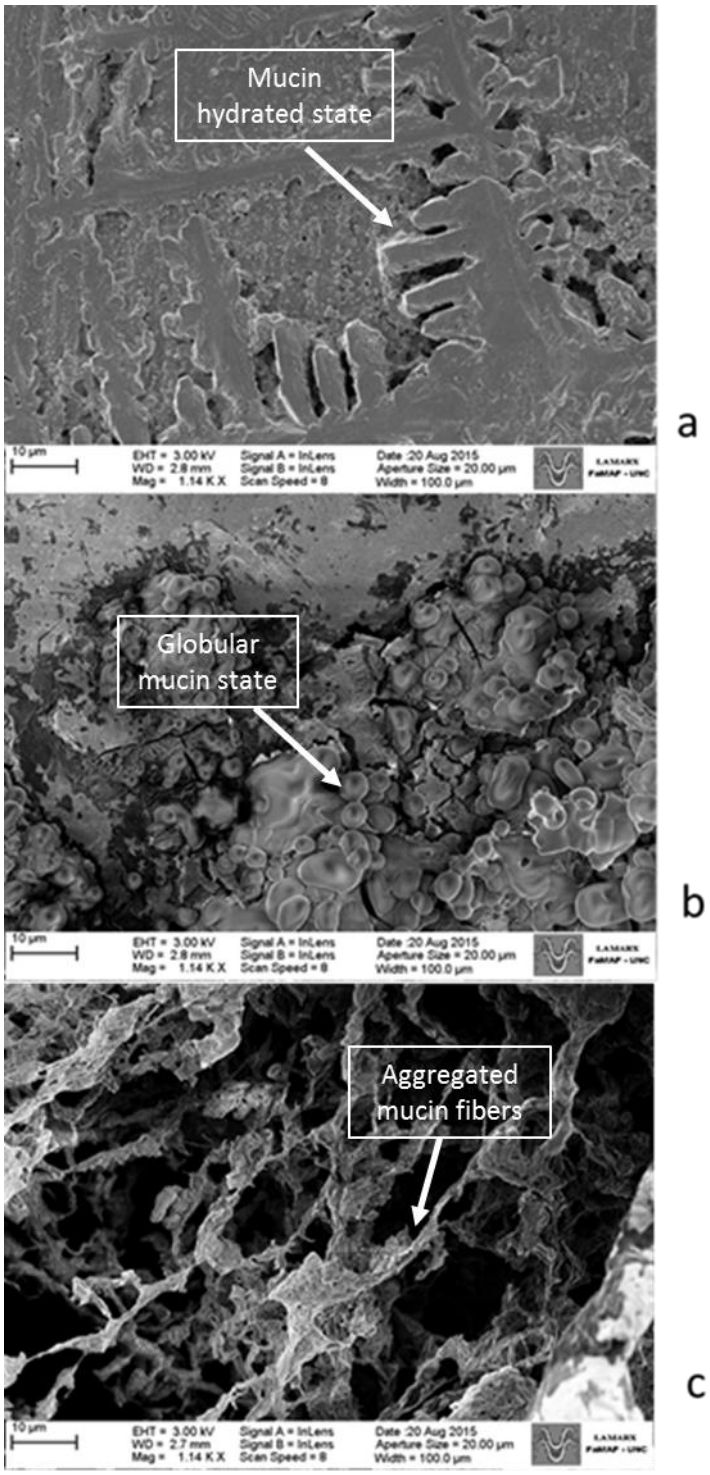

FIGURE 6

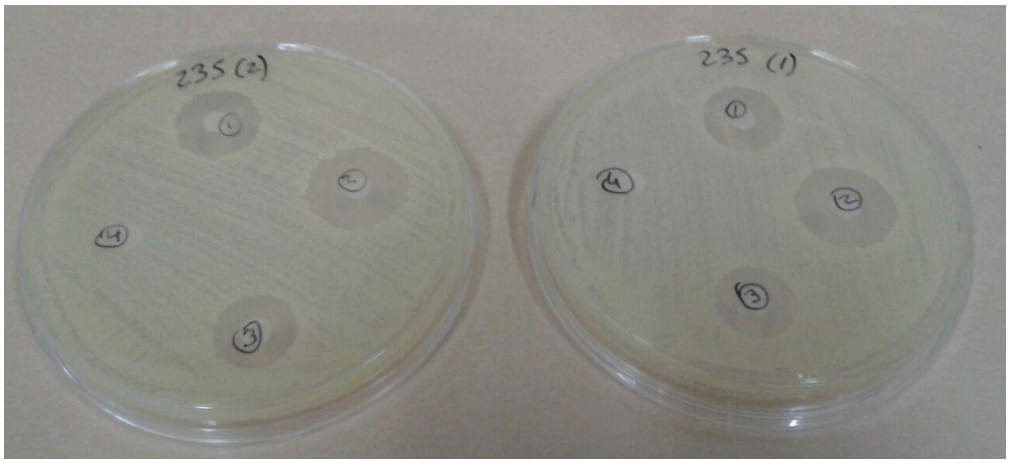

FIGURE 7

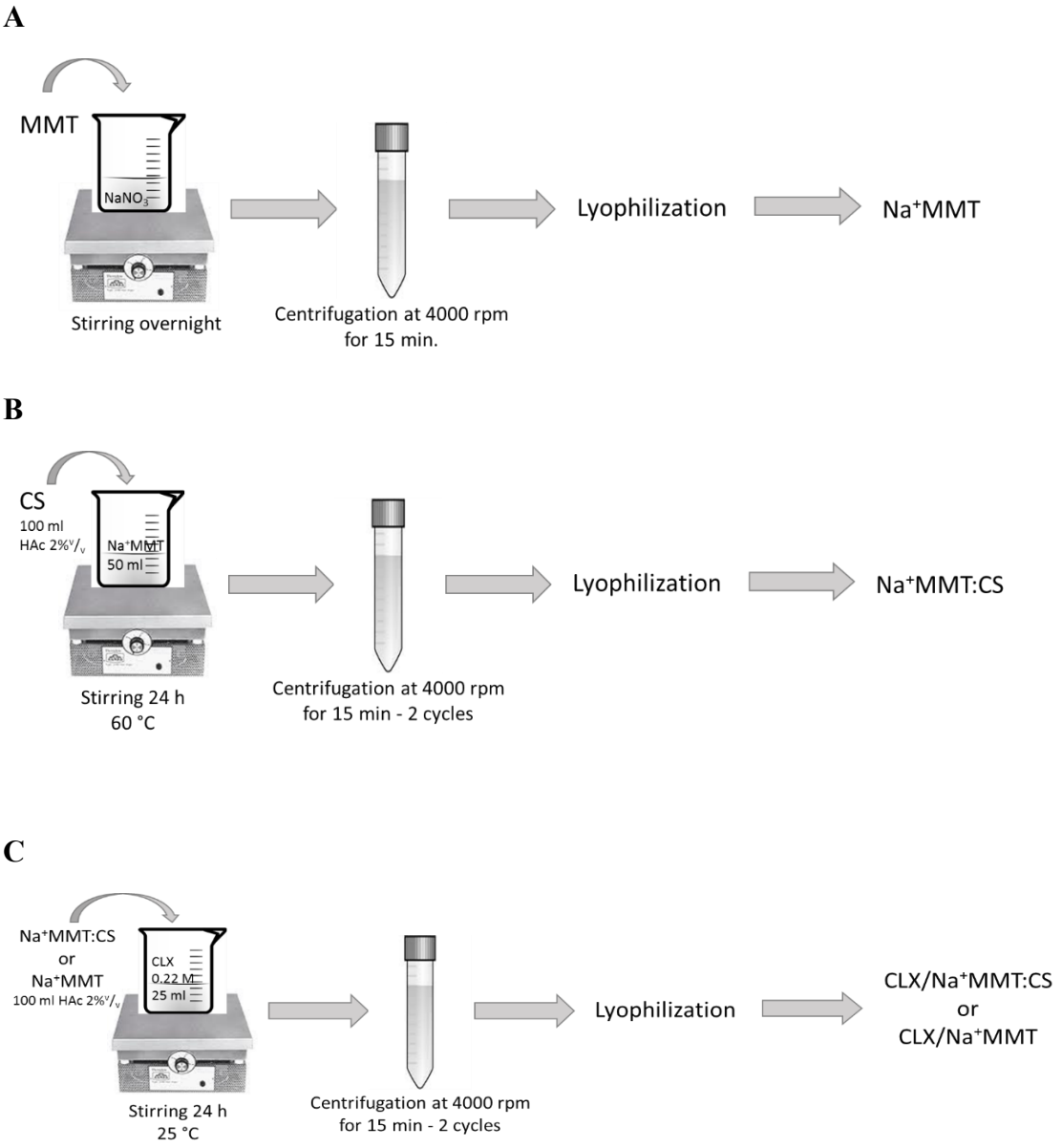

Scheme 1

Table 1. XRF-analysis of the MMT, Na^+MMT, MMT:CS and Na^+MMT:CS.

Oxides/sample	**% Mass**			
	MMT	**MMT:CS**	**Na^+MMT**	**Na^+MMT:CS**
SiO_2	77.9	69.5	71.3	63.6
AL_2O_3	14.2	14.3	13.4	14.9
Fe_2O_3	3.61	3.33	3.37	3.24
K_2O	2.06	1.76	1.97	1.58
MgO	1.29	1.51	1.94	1.12
TiO_2	0.693	0.576	0.767	0.582
CaO	0.194	0.0773	-	-
Br	0.0377	0.0086	-	-
ZrO_2	0.0356	0.0175	0.0386	0.0283
Na_2O	-	-	7.23	-
Cl	-	-	-	-
C	-	8.94	-	15.00

Table 2. Parameter *n* as estimated from the application of the Krosmeyer-Peppas model to the data of CLX formulations at different pH values (1.2, 4.1 and 6.8) and coefficient of determination (R^2).

Sample	pH	n	R^2
CLX	1.2	0.4665 ± 0.0291	0.9734 ± 0.0176
	4.1	0.4292 ± 0.0297	0.9632 ± 0.0232
	6.8	0.2237 ± 0.0432	0.8171 ± 0.0252
CLX/Na^+MMT	1.2	0.5828 ± 0.0427	0.9790 ± 0.0274
	4.1	0.6532 ± 0.0250	0.9942 ± 0.0161
	6.8	0.7365 ± 0.0334	0.9919 ± 0.0215
CLX/ Na^+MMT:CS	1.2	0.5679 ± 0.0362	0.9840 ± 0.0233
	4.1	0.6518 ± 0.0549	0.9724 ± 0.0353
	6.8	0.6640 ± 0.0457	0.9814 ± 0.0294

Table 3. Antimicrobial activity of CLX nanocomposites by disk diffusion test.

Bacterial strain	Inhibition zone ± SD (mm)			
	CLX	CLX/MTT	CLX/MMT:CS	MMT:CS
S. aureus ATCC 25923	1.2±0.1	1.4±0.1	1.2±0.1	No inhibition
S. aureus 235	1.8±0.1	2.1±0.1	1.6±0.1	No inhibition
S. aureus 787	1.8±0.1	2.1±0.1	1.6±0.1	No inhibition
S. aureus 2127	1.5±0.1	2.0±0.1	1.6±0.1	No inhibition
S. aureus 2804	1.5±0.1	2.0±0.1	1.6±0.1	No inhibition
S. aureus 123	1.5±0.1	1.9±0.1	1.6±0.1	No inhibition
S. aureus 43300	1.6±0.1	2.5±0.1	1.7±0.1	No inhibition
S. aureus 2387	1.9±0.1	2.0±0.1	1.8±0.1	No inhibition